# DEVELOPMENT OF HYBRID NANOCARRIER LIPOSOME-MESOPOROUS SILICA NANOPARTICLES BY SOLVENT INJECTION METHOD FOR PACLITAXEL DRUG DELIVERY

HIND H. ABBOOD\*, FARHAD M. OTHMAN, ALAA A. ABDUL-HAMEED

Materials Engineering Department, University of Technology- Iraq, Baghdad, Iraq \*Corresponding author email: Hind.h.abbood@uotechnology.edu.iq

### **Abstract**

This study explores hybrid Mesoporous silica nanoparticles- liposome nanocarriers as drug delivery systems for cancer therapy. It focuses on liposomecoated Mesoporous silica nanoparticles (MSNs) loaded with hydrophobic drug paclitaxel to demonstrate their potential for effective cancer treatment. The preparation and characterisation of mesoporous silica nanoparticles with two different pore sizes, small pore size and large pore sizes by modified sol-gel method, and the pore size can be modified by adding the mesitylene to MSNs. The drug loading was carried out by dissolving the pneumothorax (PTX) drug with different solvents, water, ethanol, Dimethyl sulfoxide, and dichloromethane by the Adsorption method and measuring the drug loading capacity and drug loading efficiency for both types of mesoporous silica nanoparticles. The study used a solvent injection method to introduce liposome coatings to MSNs, improving stability and biocompatibility, controlling drug release, and reducing premature leakage. All MSNs were characterised by transmission electron microscopy, Fourier transform infrared spectroscopy, N2 adsorption isotherms, scanning electron microscopy, X-ray diffraction, and z-potential analysis for determination of their characterisations. The effects of pore sizes of MSNs on the loading of PTX and its release from PTX-loaded MSNs into the in vitro drug release was carried out at two pH conditions, that is, pH = 7.4 and 5.5, as representative of physiological and cancer environment conditions. The released PTX from PTX-loaded MSNs into the pH of the physiological environment was slower than that into the cancer environment. The release of PTX was strongly pH-dependent on the selected media

Keywords: Adsorption method, Drug release, Drug delivery, Hybrid nanocarriers, Liposomes, MSN, Nanomedicine, Sol-gel method, Solvent injection method.

### 1. Introduction

Nanomedicine is an important application of nanotechnology for the prevention and treatment of diseases in humans. It is a relatively new field of technology that includes physics, chemistry, materials engineering, biology, and medical science. The practical scope of nanomedicine is ranged from 5 to 250 nm, as disclosed by Zhang et al. [1], Sahu et al. [2], and Garnett et al. [3].

Nanomedicine significantly advances targeted drug delivery, enhancing treatment effectiveness at the target site while reducing side effects. Nano-delivery systems use nanoscale carriers to address challenges such as nonspecific distribution, rapid clearance, low bioavailability, and toxicity, as explained by Samarasinghe et al. [4] and Soares et al. [5]. These systems include materials like polymeric micelles, vesicles, liposomes, hydrogels, and quantum dots, as noted by Lombardo et al. [6].

However, porous nanomaterial pores exhibit unique properties like lower density and larger surface areas, making them ideal for drug encapsulation. Wu et al. [7] categorise these materials by pore size: microporous (<2 nm), mesoporous (2-50 nm), and microporous (>50 nm). Mesoporous materials like SiO<sub>2</sub>, MgO, and TiO<sub>2</sub> are especially useful due to their high porosity and thermal characteristics (Sharma et al. [8]. MSNs, part of structured mesoporous bio-ceramics, are applied in tissue engineering, diabetes care, inflammation, and cancer treatment. Their adjustable size and large surface area make them ideal for designing nanocarriers (Iturrioz-Rodríguez et al. [9]. MSNs have low toxicity, high drug-loading capacity, and superior biocompatibility compared to other metal oxides (Kwon et al. [10]). In cancer treatment, MSNs can improve drug bioavailability and are particularly suited for delivering anti-cancer drugs like docetaxel and doxorubicin [11]. Despite these advantages, MSNs face challenges such as stability, controlled drug release, and difficulty crossing biological barriers [12]. Their large surface area can lead to faster degradation in physiological environments, raising concerns about biocompatibility [13]. According to Dua et al. [14], MSNs' interaction with red blood cells can cause homolyses, and their rapid clearance by phagocytic cells limits their circulation time.

Biomaterials such as lipids, micelles, dendrimers, liposomes, and polymeric carriers like hydrogels offer biodegradable and biocompatible solutions. However, they have limitations, including stability issues, lack of controlled release, and difficulty in overcoming biological barriers [15]. The combination of nanocarriers, such as coating MSNs with liposomes, can improve stability, biocompatibility, and targeted drug delivery to tumours, as suggested by Laffleur and Keckeis [16]. Huang et al. [17] also demonstrated that coating MSNs with liposomes can reduce premature drug release and enhance delivery to tumour sites. Paclitaxel (Taxol) is a successful anti-cancer drug, traditionally requiring solvents that cause side effects. Nano-formulations of paclitaxel eliminate the need for these solvents, improving its delivery and reducing side effects [18-20]. MSNs, synthesised via the sol-gel method [21], can be loaded with paclitaxel through adsorption, allowing effective release in both physiological and cancer environments [22].

The objective of the study is to explore the features of hybrid mesoporous silica nanoparticles- liposome (MSNs-LIP) nanocarriers as drug delivery systems for cancer therapy. It focuses on liposome-coated MSNs loaded with hydrophobic drug paclitaxel to demonstrate their potential for effective cancer treatment. Two types of

MSNs, small and large pores, with acceptable surface area and appropriate pore sizes, have been synthesised successfully by sol-gel method using etraethyl orthosilicate as a source of silica, CTAB surfactant, and mesitylene as pores expender. The product has been subjected to a wide range of tests and characterisations.

### 2. Experimental Methodology

### 2.1. Synthesis of MSN with different pore sizes

Two types of small mesoporous silica nanoparticles (S-MSNs) and large (L-MSNs) pores were prepared with a little modification following standard procedure. For S-MSNs, the solution of 480 mL deionised water and NaOH (aq) (2M, 3.5 mL), (1.0 g, 2.7 mmol) of Cetyltrimethylammonium bromide (CTAB) was vigorously stirred at 1000 rpm for 5 hours at 80 °C in the bottom round flask. Then, 5.0 mL, 22.56 mmol dropwise tetraethyl orthosilicate was added by pipette at a rate of 1.0 mL/min, and the mixture was vigorously stirred for another 2 hours at 80 °C. The resulting white precipitate was filtered by a vacuum filter, washed with plenty of methanol to remove partial surfactant, and dried at room temperature. For L-MSNs, 7.0 mL 50.30 mmol of mesitylene was added to the solution with CTAB, which expanded the pores of MSNs for 1, 2, and 5 hours. Then, by using the Calcination in the furnace, the surfactant template was removed at 550 °C for 6 hr. with a heating rate of 1-2 °C /min. Lastly, white powder was produced of S-MSNs and L-MSNs.

### 2.2. Drug loading

For PTX loading, an Adsorption method was utilised. Drug loading is commonly accomplished by soaking a drug solution with MSNs to allow adsorption through interaction between the drug and the particle surface. This interaction is mediated through hydrogen bonding and electrostatic attractions. Before using MSNs for drug loading, 200 mg of S-MSNs and L-MSNs were kept in the oven at 80°C for 30 min to remove the moisture from the Mesostructure's pores to obtain maximum saturation for PTX loading. PTX solution is prepared by dissolving 100 mg of PTX with 10 ml of different solvents, water, ethanol, Dimethyl sulfoxide (DMSO), and dichloromethane in a sonicator to obtain clear, concentrated drug solutions. After that, S-MSNs and L-MSNs were soaked with paclitaxel solution for drug loading after agitating under closed and light-sealed conditions for different intervals of 1, 2, 4, 8, 16, and 24 hours at 25 °C and 400 rpm.

The supernatants were measured with High-performance liquid chromatography (HPLC) to assess the amount of unentrapped drug. Drug-loaded MSNs were centrifuged at 10,000 rpm for 30 minutes, washed with deionised water to remove res, and separated again with 4 centrifuge devices. The product was then dried in a vacuum furnace, resulting in the white powder from PTX@S-MSNs and PTX@L-MSNs.

PTX loading efficiency(LE%) = 
$$\frac{\text{(Total PTX - unloaded PTX)}}{\text{Total [PTX]}} \times 100$$
 (1)

PTX loading capacity(LC%) = 
$$\frac{\text{(Total PTX - unloaded PTX)}}{\text{amount of PTX loaded in MSNs}} \times 100$$
 (2)

# 2.3. Coating mesoporous silica nanoparticles with liposome

The coating of mesoporous silica nanoparticles with liposome by Solvent injection methods. 200 mg of DPPC and 100 mg cholesterol were dissolved in 25 ml of

ethanol and added drop by drop to 50 ml of warm aqueous solution (water) of S MSNs or L-MSNs (200 mg per 50 mL) at 60 °C with stirring. The solution turned to milky form as the formation of liposomes then stirring was continued for 24 hr in the dark. The coated S-MSNs and L-MSNs were Centrifuged at 10,000 rpm for 20 minutes, then dried at 40 °C for 8 hours. The white powder was formed and collected in a sealed vial for further tests and experiments of release.

### 2.4. MSNs characterisation

Various instruments were used for nanoparticle characterisation. SEM (FEI INSPECT F50) analysed the structure and morphology of S-MSNs and L-MSNs, while EDX confirmed the absence of CTAB and mesitylene in the samples. The specific surface area and total pore volume were measured using nitrogen adsorption isotherms (BET method). XRD (Panalytical X'Pert) identified crystalline structures and phases, and TEM confirmed the porous framework and particle size. FT-IR, brand Thermo Fisher Scientific, was used to analyse chemical bonds, and zeta potential was measured using Zeta Sizer Nano ZS. HPLC (Knauer, Germany) was employed for separating, identifying, and quantifying compounds, using a C18 column with a UV detector at 228 nm for drug loading and release studies.

# 2.5. In vitro drug release study

### 2.5.1. Standard calibration curve preparation

The calibration curves for PTX were established using a methanol solution. A stock solution with a concentration of 2 mg/ml was prepared, and from this, a series of PTX dilutions with varying concentrations ranging from 1 to 200 µg/ml were created. PTX detection was performed by matching the retention time and absorbance spectrum of each PTX standard. HPLC analysis was conducted at the wavelength corresponding to the maximum absorbance of PTX ( $\lambda$  max = 228 nm). The concentration of PTX in the samples was determined by relating the serial concentrations of external standard materials to their respective peak with the construction of a calibration curve correlating concentration with peak area.

# 2.5.2. In-vitro drug release

In vitro drug release was studied using two PBS solutions of 7.4 and 5.5 potential of hydrogen (*pH*) containing 0.1% Tween 80 to improve PTX solubility. PTX@S-MSNs, PTX@L-MSNs, LIP-PTX@S-MSNs, and LIP-PTX@L-MSNs (5 mg) were suspended in 15 ml PBS and shaken at 100 rpm, 37 °C. Samples were taken at intervals of 10, 20, and 30 minutes, 1, 2, 4, 8, 16, and 24 hours, centrifuged at 16,000 rpm for 30 minutes, and supernatants were analysed via HPLC. MSNs were redispersed in PBS after each sampling for continued analysis, enabling accurate drug release measurement over time.

## 3. Results and Discussion

### 3.1. Standard calibration

Figure 1 shows the calibration curve of PTX in dichloromethane. The plotting of area against concentrations resulted in a straight line. The square correlation

coefficient  $R^2$  was found to be 0.9973. This means that the calibration curve complied with the law of Beer in the range of concentrations used.

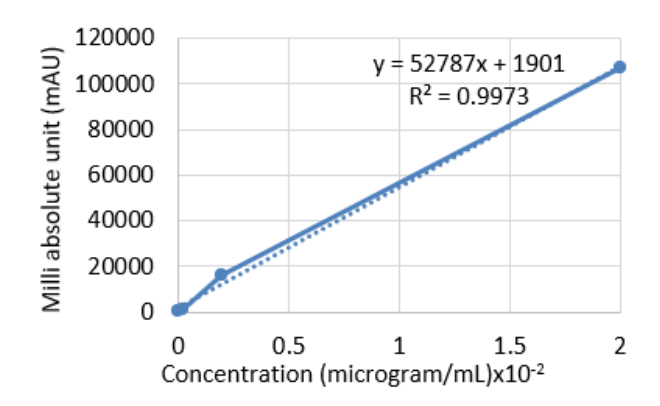


Fig. 1. Calibration curve of PTX in methanol by HPLC.

### 3.2. Characterisation

# 3.2.1. Scanning electron microscopy and energy dispersive X-ray analysis

EDX analysis, displayed in Fig. 2, confirmed the chemical composition, showing characteristics of silicon and oxygen peaks in both S-MSNs and L-MSNs samples. The atomic and weight ratios of silicon and oxygen were listed in Tables 1 and 2, with a gold peak attributed to the sample coating process before the EDX test.

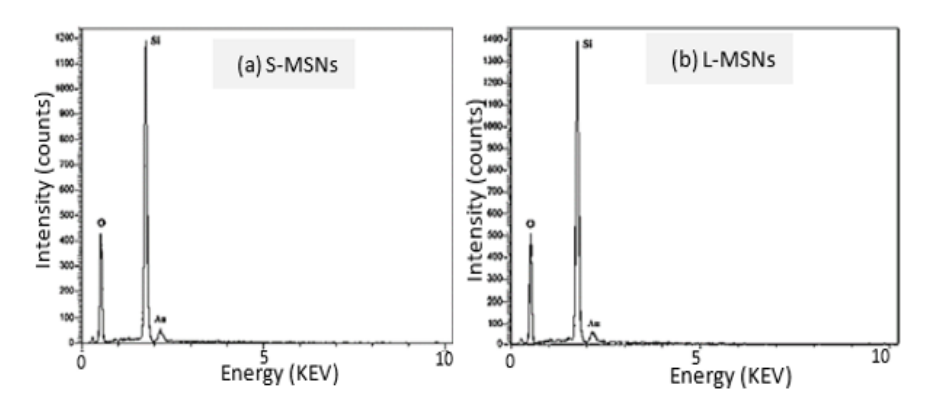


Fig. 2. EDX spectra of prepared mesoporous silicon of S-MSNs and L-MSNs.

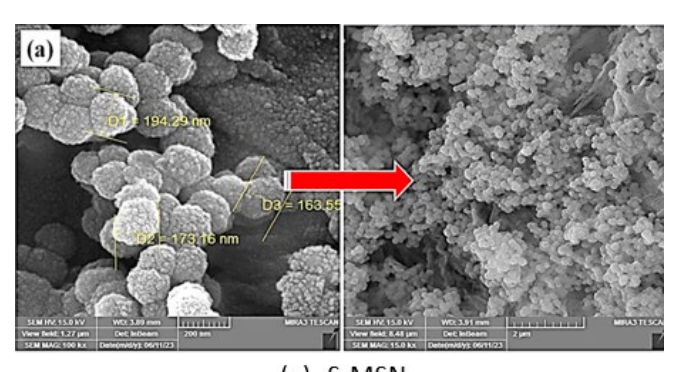
Table 1. The element ratios of small mesoporous silicon, S-MSNs.

Element	Weight (%)	Atomic (%)	Error (%)
0	53.01	66.45	2.0184
Si	46.99	33.55	2.7402
Total	100.00	100.00	
percentage			

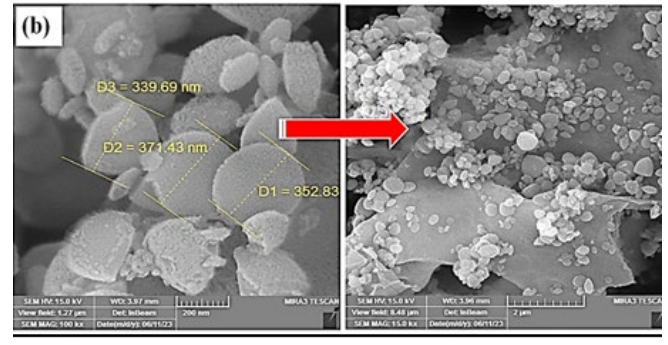
Table 2. The element ratios of large mesoporous silicon, L-MSNs.

Element	Weight (%)	Atomic (%)	Error (%)
0	53.30	66.71	1.5035
Si	46.70	33.29	2.5435
Total percentage	100.00	100.00	

The surface morphology of synthesised S-MSN and L-MSN nanoparticles was studied using scanning electron microscopy (SEM), as depicted in Fig. 3. SEM images revealed nearly spherical silica nanoparticles with an average size of 177 nm and a rough, porous surface, as shown in Fig. 3(a). Adding mesitylene increased particle size to 354.65 nm and made surfaces rougher, as shown in Fig. 3(b), indicating mesitylene's impact on size and shape.







(b) L-MSN.

Fig. 3. scanning electron microscopy images of porous silica nanoparticles

## 3.2.2. Transmission electron microscopy (TEM)

Transmission Electron Microscopy (TEM) was used to examine the morphology of the samples. Figures 4(a), 4(b), 5(a), and 5(b) show TEM images of S-MSNs, coated S-MSNs, L-MSNs, and coated L-MSNs, respectively. The nanoparticles were spherical and mono-distributed, with particle sizes of 30 nm for S-MSNs and 58 nm for L-MSNs. The images revealed a honeycomb-like porous structure, with hollow pores visible in uncoated samples (light-coloured) and filled pores in coated samples

(dark-coloured), indicating successful deposition of liposome material on the mesoporous silica. Hexagonally packed channels were clearly observed in Fig. 5(b).

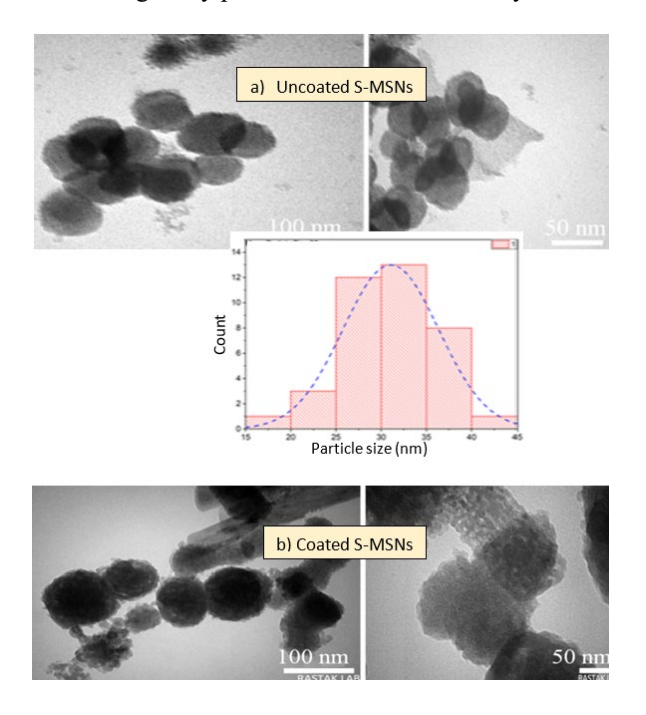


Fig. 4. Transmission electron microscopy (TEM) images of prepared uncoated and coated small mesoporous silicon nanoparticles.

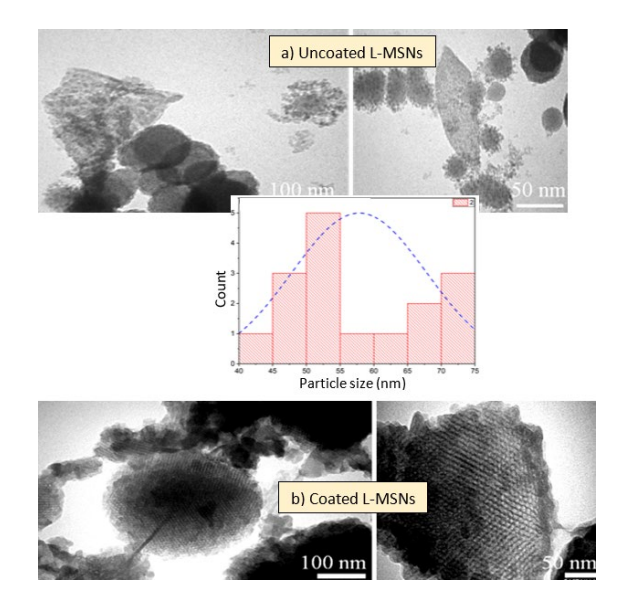


Fig. 5. Transmission electron microscopy (TEM) images of prepared uncoated and coated large mesoporous silicon nanoparticles.

## 3.2.3. BET/BJH analyser

Nitrogen adsorption-desorption analysis was used to study the porosity of MSNs. Before characterisation, a single sample was degassed for 5 hours at 200 °C under vacuum. Barrett-Joyner-Halenda (BJH) method is used to study the pore size distribution of porous materials in micropores and mesopores. BET-specific surface area, pore volume, and pore diameter were measured using the BET and BJH methods. Figures 6(a) and 6(b) show the nitrogen adsorption-desorption isotherms of S-MSNs and L-MSNs, both displaying type IV isotherms with a hysteresis loop at high pressure, P/Po = 0.8 - 1, characteristic of mesoporous materials.

The hysteresis loop of samples at relative pressure of P/Po = 0.3 - 0.8 matches type H1, indicating cylindrical pores, while at higher pressure, it shifts to type H3, signifying slit-shaped pores. This mixture is due to the surfactant CTAB forming both spherical and oblate micelles. Adsorption curves show knees above P/Po = 2.2, corresponding to capillary condensation. The specific surface area of S-MSNs ( $424.27 \text{ m}^2/\text{g}$ ) is smaller than that of L-MSNs ( $686.84 \text{ m}^2/\text{g}$ ), with pore sizes of 2.5 nm and 3.2 nm, respectively as shown in Fig. 7. Both samples exhibit type H1 followed by H3 loops, showing that mesopores are maintained despite some shrinkage (Richman et al. [23]; Kim et al. [24]).

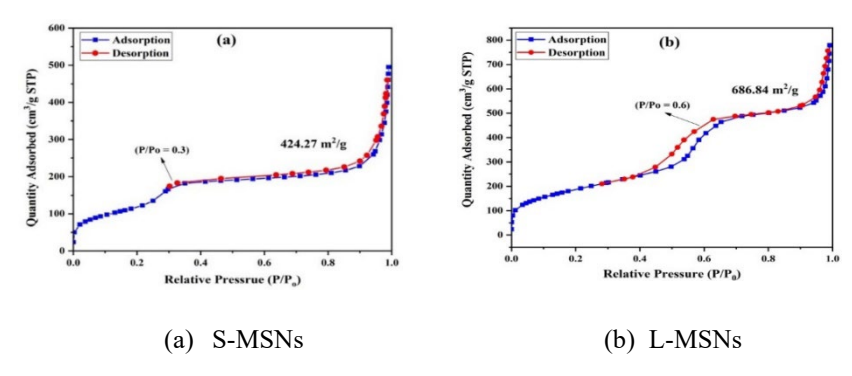


Fig. 6. Brunauer–Emmett–Teller (BET) (surface area analysis): Nitrogen adsorption-desorption isotherm curves of S-MSNs and L-MSNs samples.

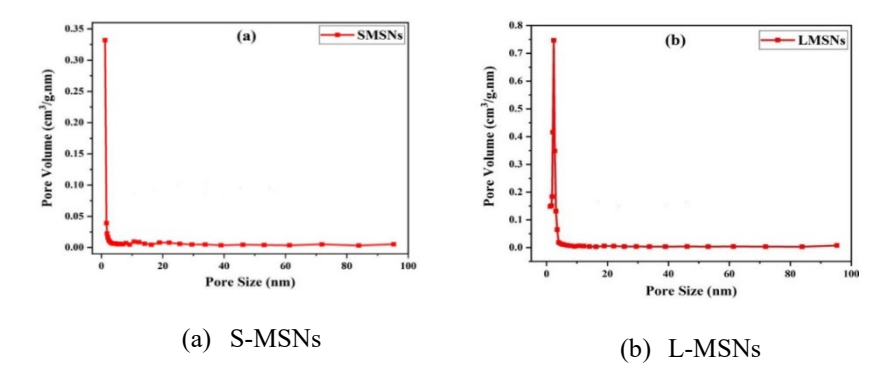


Fig. 7. BJH pore volume vs. pore size curves (BET) of S-MSNs and L-MSNs samples.

# 3.2.4. X-ray diffraction results

XRD was carried out to determine the crystalline structure of prepared porous silicon samples using a Shimadzu XRD-6000 powder diffractometer. Figure 8 shows the XRD patterns of pure and PTX-loaded porous silicon samples. The obtained XRD patterns confirmed the amorphous crystalline structure of all pure and PTX-loaded silicon samples. The results showed that the XRD patterns of all samples with a broad peak at  $2\Theta = 22.1^{\circ}$ , which attributed to the amorphous structure of silica nanoparticles, corresponded to the standard data (96-101-0939), the XRD patterns agreed with the SEM and TEM results. There is no noticeable difference detected between the XRD patterns for pure and PTX-loaded samples, which indicated similar structures of silica nanoparticles [25, 26].

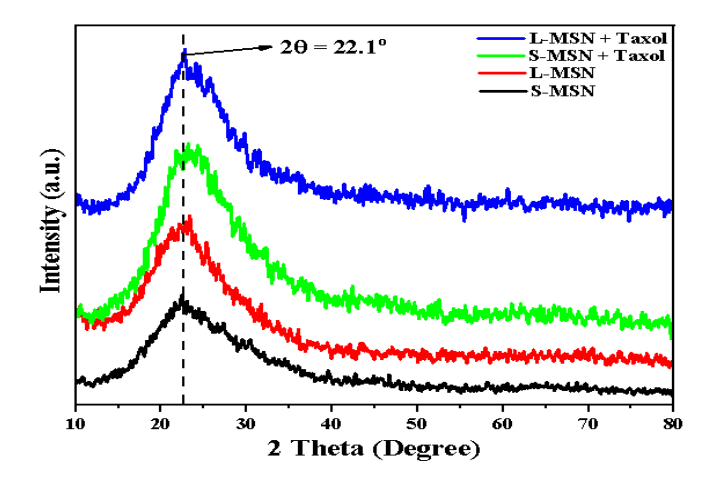


Fig. 8. XRD patterns of prepared porous silica nanoparticle samples, S-MSN, L-MSN, PTX@S-MSNs, and PTX@L-MSNs.

## 3.2.5. Fourier-transformed infrared spectra results

The FTIR spectroscopy test was carried out to determine the functional groups within the prepared porous silica samples using an FTIR spectrometer type SHIMADZU - FTIR 8400 in the range of 500 – 4000 cm<sup>-1</sup>. Figures 9 and 10 presented the obtained FTIR spectra curves of S-MSNs and L-MSNs samples. The examined samples were pure S/LMSNs, loaded PTX-S/LMSNs and then coated LIP-PTX@S/LMSNs. The results in Figs. 8(a) and 9(a) show a strong absorption band at 1050 cm<sup>-1</sup>, attributed to Si-O-Si bond stretching, with a shoulder at 984 cm<sup>-1</sup>, and other bands at 708 cm<sup>-1</sup>, 800 cm<sup>-1</sup>, 2345 cm<sup>-1</sup>, and 3409 cm<sup>-1</sup> related to Si-H bond deformation [27, 28]). Paclitaxel's characteristic bands at 1712 cm<sup>-1</sup> and 1648 cm<sup>-1</sup> (C = O and C-C stretching) were confirmed (according to Ha et al. [29]). FTIR spectra of PTX-loaded MSNs showed an increase in the Si-O-Si bandwidth due to overlap with paclitaxel bands at 1245 cm<sup>-1</sup> and 1074 cm<sup>-1</sup> [30]. Liposome coating introduced new bands at 1471 cm<sup>-1</sup>, 1730 cm<sup>-1</sup>, 2853 cm<sup>-1</sup>, and 2910 cm<sup>-1</sup>, indicating successful encapsulation [31]. Peaks at 708 cm<sup>-1</sup> and 984 cm<sup>-1</sup> became sharper after adding PTX and liposomes, with no major differences between large and small MSNs.

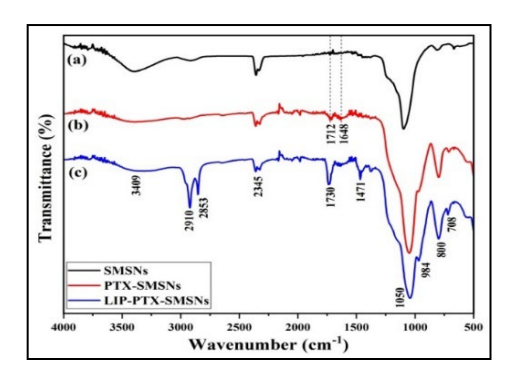


Fig. 9. FTIR spectra curves of prepared samples (a) S-MSNs (b) PTX@S-MSNs (c) LIP-PTX@S-MSNs.

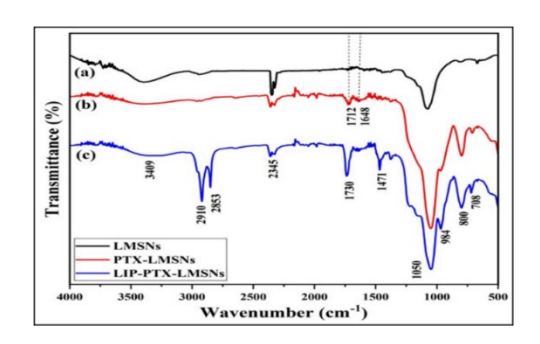


Fig. 10. FTIR spectra curves of prepared samples (a) L-MSNs (b) PTX@L-MSNs (c) LIP-PTX@L-MSNs.

### 3.2.6. Zeta potential analyser results

Zeta potential is crucial for confirming successful nanoparticle coating, as it changes during each fabrication step. It reflects surface charge and stability, helping to understand nanoparticle interactions. According to Jin et al. [32], a high positive or negative zeta potential indicates particle repulsion, preventing aggregation. The zeta potential of prepared samples was measured in deionised water to assess electric potential and surface charge, and the measurement results are presented in Table 3. Results showed MSNs generally had a negative charge due to the silanol group (Si-OH). PTX-loaded MSNs showed increased zeta potential due to the positive charge from carboxyl and amine groups of PTX, reducing the overall negative charge. Liposome-coated MSNs had a negative charge due to the hydrophilic heads and cholesterol's hydroxyl group [33-35].

Table 3. zeta potentials of four prepared samples, S-MSNs, S-SMNs loaded PTX, L-MSNs, ad L-MSNs loaded PTX.

Sample	Zeta Potential (mV)
S-MSNs	-19.63
S-MSNs loaded PTX	56.52
L-MSNs	-1.2
L-MSNs loaded PTX	19.32

# 3.3. Drug loading

The MSNs appeared to have accessible mesopores, as indicated in TEM images and N2 adsorption-desorption analyses. Hence, they were used as drug carriers for the water-insoluble drug PTX using the adsorption method. The loading of PTX into the MSNs is also controlled by the chemical nature of the size, pores, and shape of the nanoparticles may be related to electrostatic interactions. The inorganic networks of MSNs have a large number of silanol groups (Si-OH), which interact with the functional group of PTX drug by means of hydrogen bonding on the mesopore surface. Interaction between the MSNs silanol group and the drug functional group was attractive. The drug molecules are either confined within the pores or adsorbed to the surface of MSNs. The probable mechanism of drug loading is that the H group of amine or carboxyl and hydroxyl group of PTX will form hydrogen bonds to the group of silanol mesoporous silica nanoparticles, and the drug molecules will then be retained in the mesopores. Due to liposome work as capping to protect the drug from premature release, PTX was released gradually from MSNs, with a much lower but steady release rate after 4 hrs.

## 3.3.1. Effect of solvent loading

MSNs' high loading capacity is due to their adsorptive properties and large pore volume, allowing them to load both hydrophilic and hydrophobic drugs. Solvents like water, ethanol, DMSO, and dichloromethane were tested for loading the hydrophobic PTX. As shown in Table 4, the drug loading increased as solvent polarity decreased, with dichloromethane showing the highest loading of 24.6%, likely because its low polarity did not compete with PTX for MSN absorption.

Table 4. Loading capacity at unferent solvents.		
Solvent	polarity	Loading capacity (%)
Water	10.2	10.2
Ethanol	7.8	11.6
DMSO	7.2	22.8
Dichloromethane	3.4	24.6

Table 4. Loading capacity at different solvents.

# 3.3.2. Drug loading periods

Different drug loading periods of 1, 2, 4, 8, 16, and 24 hr at 25 °C and 400 rpm were utilised to determine the optimal time for PTX loading and investigate the adsorption equilibrium time of the drug when the drug loading processed in dichloromethane for both S-MSNs and L-MSNs. As depicted in Fig. 11, the drug loading content gradually increased with the increase of the loading period within 6 hr, about 18.6% for S-MSNs and 24.6% for L-MSNs. As the loading period increased to 24 h, the drug loading content still stayed constant, indicating that drug adsorption on the surface of MSN had reached equilibrium at 6 hr; hence, the optimal drug loading time was 6 hr.

The loading of PTX was driven by diffusion where, due to concentration gradient, PTX diffused into a porous structure with lower concentration from a bulk of solution with higher concentration. A load of drugs with MSNs depends on the size of the pore. The PTX loading capacity (PTX/LC) and the PTX loading efficiency (PTX/LE)

were calculated using an HPLC as two types of MSNs calculated with the help of the calibration curve for the investigation of the carriers' ability.

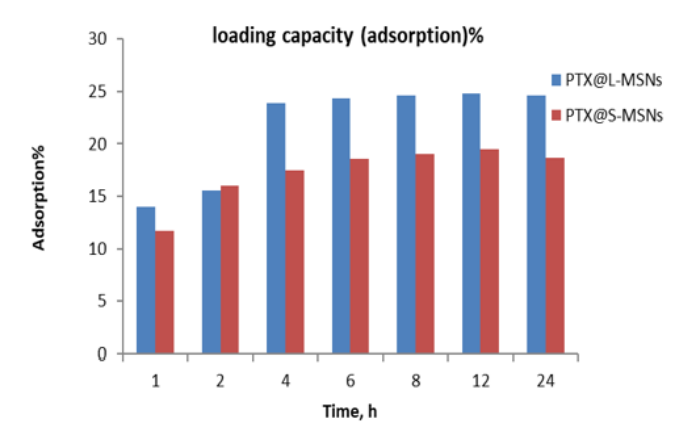


Fig. 11. Effect of period time on loading capacity.

As shown in Table 5, LC% in L-MSNs is greater than S-MSNs because the surface area of S-MSNs is smaller than L-MSNs and of the larger size of L-MSNs, which provided much more free hydroxyls group than S-MSNs, capable of forming hydrogen bonds with the PTX. he improved dissolution of PTX from mesoporous silica nanoparticles is the crystal transition from ordered to disordered caused by spatial confinement within a nanosized pore.

Table 5. MSN loading efficiency and loading capacity percentage in dichloromethane.

Nanocarriers	Loading efficiency (%)	Loading capacity (%)
L-MSNs	21	24.6
S-MSNs	10.4	18.6

## 3.4. In vitro drug release

To investigate the drug release profile of PTX@S-MSNs, PTX@L-MSNs, LIP-PTX@S-MSNs, and LIP-PTX@L-MSNs have been compared with free PTX, the in vitro drug release was carried out at two pH conditions, pH = 7.4 and 5.5 as representative of physiological and cancer environment conditions. This was studied in PBS containing 0.1% (v/v) Tween 80 at 37 °C. All the release rates of PTX from loaded MSNs were much faster than those of pure drugs.

Figure 12 shows that drug release from PTX@S-MSNs, PTX@L-MSNs, LIP-PTX@S-MSNs, and LIP-PTX@L-MSNs follows a biphasic pattern with an initial burst, beneficial for quickly reaching effective concentrations, followed by a prolonged release. The burst release comes from PTX in the external pores, while the slower release is from PTX inside the MSNs. At pH 7.4, drug release after 8 hours was 37%, 33%, 25%, and 19%, respectively, for the different formulations. At pH 5.5, release rates were higher, indicating the system's *pH*-sensitive nature, ideal for targeting acidic tumour environments and minimising side effects in normal tissues. This pH-sensitive mechanism improves the efficiency of cancer treatment by preventing premature drug release.

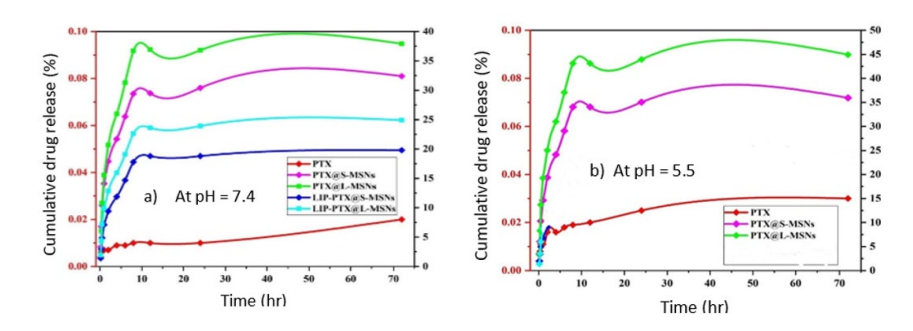


Fig. 12. PTX release from samples at pH equal to a: 7.4, b: 5.5.

# 4. Conclusions

Two types of ordered MSNs (small and large pores), with acceptable surface area and appropriate pore sizes, have been synthesised successfully by sol-gel method using tetraethyl orthosilicate as a source of silica, CTAB surfactant, and mesitylene as pores expender. The characterisation of the developed MSNs revealed that the monodispersed MSNs have a specific surface area for S-MSNs of 424.27 m²/g and L-MSNs of 686.84 m²/g. The pore size of S-MSNs and L-MSNs was 2.5 nm and 3.2 nm, respectively.

It is found that the drug loading capacity increases with the decreasing of the solvent polarity parameter. Also, the drug loading capacity of PTX increases with increasing contact time. After 6 hours, it has become almost constant for both S-MCMs and L-MCMs dosage, and maximum drug loading efficiency for PTX for SMSNs and LMSMs are 24% and 18.6%, respectively. The PTX release from MSNs without coating in pH 5.5 and pH 7.4 was faster than MSNs with coating liposomes. The PTX release in acidic media at pH 5.5 is better than pH 7.4 and, as a result, reduces side effects from the drug. Since tumour tissue is more acidic than normal tissue but may be released to improve treatment in tumour tissues. The prepared MSNs were effectively provided with the ability to encapsulate antitumor drug PTX with high load capacity in their mesopores.

Recommendations for future studies include developing methods to control PTX release from MSNs and investigating their pharmacokinetics, biodistribution, and clinical safety in vivo. Further research should focus on synthesising different mesoporous nanoparticles (e.g., MgO, ZrO2, TiO2, and geopolymer) for drug delivery, coating with various materials, and testing hydrophilic drugs. Hybrid nanocarriers could be synthesised for medical applications such as antimicrobial and antibacterial activities. Future studies should also perform cell viability, uptake, apoptosis, and haemolysis assays for liposome-coated MSNs.

Nomenclatures		
pН	Potential of hydrogen	
Abbreviations		
DMSO	Dimethyl Sulfoxide	
FTIR	Fourier Transform Infrared Spectroscopy	

L-MSNs	Large Mesoporous Silica Nanoparticles
MSNs	Mesoporous Silica Nanoparticles
PTX	Pneumothorax
SEM	Scanning Electron Microscopy
S-MSNs	Small Mesoporous Silica Nanoparticles
TEM	Transmission Electron Microscopy

### References

- 1. Zhang, C. et al. (2020). Progress, challenges, and the future of nanomedicine. *Nano Today*, 35, 101008.
- Sahu, T. et al. (2021). Nanotechnology based drug delivery system: Current strategies and emerging therapeutic potential for medical science. *Journal of Drug Delivery Science and Technology*, 63, 102487.
- 3. Garnett, M.C.; and Kallinteri, P. (2006). Nanomedicines and nanotoxicology: Some physiological principles. *Occupational Medicine*, 56(5), 307-311.
- 4. Samarasinghe, R.M.; Kanwar, R.K.; and Kanwar, J.R. (2012). The role of nanomedicine in cell-based therapeutics in cancer and inflammation. *International Journal of Molecular and Cellular Medicine*, 1(3), 133.
- 5. Soares, S.; Sousa, J.; Pais, A.; and Vitorino, C. (2018). Nanomedicine: Principles, properties, and regulatory issues. *Frontiers in Chemistry*, 6, 360.
- Lombardo, D.; Kiselev, M.A.; and Caccamo, M.T. (2019). Smart nanoparticles for drug delivery application: development of versatile nanocarrier platforms in biotechnology and nanomedicine. *Journal of Nanomaterials*, 2019(10), 3702518.
- 7. Wu, L.; Li, Y.; Fu, Z.; and Su, B.-L. (2020). Hierarchically structured porous materials: Synthesis strategies and applications in energy storage. *National Science Review*, 7(11), 1667-1701.
- 8. Sharma, A.; Vaghasiya, K.; and Verma, R.K. (2016). Inhalable microspheres with hierarchical pore size for tuning the release of biotherapeutics in lungs. *Microporous and Mesoporous Materials*, 235, 195-203.
- 9. Iturrioz-Rodríguez, N.; Correa-Duarte, M.A.; and Fanarraga, M.L. (2019). Controlled drug delivery systems for cancer based on mesoporous silica nanoparticles. *International Journal of Nanomedicine*, 14(2019), 3389-3401.
- 10. Kwon, S. et al. (2013). Silica-based mesoporous nanoparticles for controlled drug delivery. *Journal of Tissue Engineering*, 4, 2041731413503357.
- 11. Guleria, M.; Thakur, P.; Chhetri, J.; and Sudhakar, K. (2021). Mesoporous silica nanoparticles as a flexible drug delivery system: Road map to targeted and controlled release formulation. *PENSEE*, 51(1), 781-809.
- 12. Jadhav, K.S.; Dumbare, P.S.; and Pande, V.V. (2015). Mesoporous silica nanoparticles (MSN): A nanonetwork and hierarchical structure in drug delivery. *Journal of Nanomedicine Research*, 2(5), 1-8.
- 13. Vallet-Regí, M.; Colilla, M.; Izquierdo-Barba, I.; and Manzano, M. (2017). Mesoporous silica nanoparticles for drug delivery: Current insights. *Molecules*, 23(1), 47.

- 14. Dua, J.S.; Rana, A.C.; and Bhandari, A.K. (2012). Liposome: Methods of preparation and applications. *International Journal of Pharmaceutical Studies and Research*, 3(2), 14-20.
- 15. Madni, A. et al. (2017). *Hybrid Nanocarriers for potential drug delivery*. In Maiti, S.; and Sen, K.K. (Eds.), *Advanced Technology for Delivering Therapeutics*, Intech Rijeka, Croatia, 54-87.
- 16. Laffleur, F.; and Keckeis, V. (2020). Advances in drug delivery systems: Work in progress still needed? *International Journal of Pharmaceutics*, 590, 119912.
- 17. Huang, R. et al. (2020). Mesoporous silica nanoparticles: Facile surface functionalisation and versatile biomedical applications in oncology. *Acta Biomaterialia*, 116, 1-15.
- 18. Ezrahi, S.; Aserin, A.; and Garti, N. (2019). Basic principles of drug delivery systems—the case of paclitaxel. *Advances in Colloid and Interface Science*, 263, 95-130.
- 19. Alves, R.C.; Fernandes, R.P.; Eloy, J.O.; Salgado, H.R.N.; and Chorilli, M. (2018). Characteristics, properties and analytical methods of paclitaxel: A review. *Critical reviews in Analytical Chemistry*, 48(2), 110-118.
- 20. Raza, F. et al. (2022). Recent advances in the targeted delivery of paclitaxel nanomedicine for cancer therapy. *Materials Advances*, 3(5), 2268-2290.
- 21. Ghaferi, M. et al. (2021). Mesoporous silica nanoparticles: Synthesis methods and their therapeutic use recent advances. *Journal of Drug Targeting*, 29(2), 131-154.
- 22. Seljak, K.B.; Kocbek, P.; and Gašperlin, M. (2020). Mesoporous silica nanoparticles as delivery carriers: An overview of drug loading techniques. *Journal of Drug Delivery Science and Technology*, 59, 101906.
- 23. Richman, E.K.; Kang, C.B.; Brezesinski, T.; and Tolbert, S.H. (2008). Ordered mesoporous silicon through magnesium reduction of polymer templated silica thin films. *Nano Letters*, 8(9), 3075-3079.
- 24. Kim, K.H. et al. 2015). Complete magnesiothermic reduction reaction of vertically aligned mesoporous silica channels to form pure silicon nanoparticles. *Scientific Reports*, 5(1), 9014.
- 25. Nguyen, V.-H.; Vu, C.M.; Choi, H.J.; and Kien, B.X. (2019). Nanosilica extracted from hexafluorosilicic acid of waste fertiliser as reinforcement material for natural rubber: Preparation and mechanical characteristics. *Materials*, 12(17), 2707.
- 26. Nguyen-Thi, N.-T. et al. (2019). The engineering of porous silica and hollow silica nanoparticles to enhance drug-loading capacity. *Processes*, 7(11), 805.
- 27. Lucovsky, G.; Yang, J.; Chao, S.S.; Tyler, J.E.; and Czubatyj, W. (1983). Oxygen bonding environments in glow-discharge-deposited amorphous silicon-hydrogen alloy films. *Physical Review B*, 28(6), 3225.
- 28. Gupta, P.; Dillon, A.C.; Bracker, A.S.; and George, S.M. (1991). FTIR studies of H2O and D2O decomposition on porous silicon surfaces. *Surface Science*, 245(3), 360-372.
- 29. Ha, P.T. et al. (2016). Targeted drug delivery nanosystems based on copolymer poly (lactide)-tocopheryl polyethylene glycol succinate for cancer treatment. *Advances in Natural Sciences: Nanoscience and Nanotechnology*, 7(1), 015001.

- 30. Devi, T.S.R.; and Gayathri, S. (2010). FTIR and FT-Raman spectral analysis of paclitaxel drugs. *International Journal of Pharmaceutical Sciences Review and Research*, 2(2), 106-110.
- 31. Mudakavi, R.J.; Raichur, A.M.; and Chakravortty, D. (2014). Lipid coated mesoporous silica nanoparticles as an oral delivery system for targeting and treatment of intravacuolar Salmonella infections. *RSC Advances*, 4(105), 61160-61166.
- 32. Jin, H.; Ansari, M.B.; and Park, S.E. (2011). Mesoporous MFI zeolites by microwave induced assembly between sulfonic acid functionalised MFI zeolite nanoparticles and alkyltrimethylammonium cationic surfactants. *Chemical Communication*, 47(26), 7482-7484.
- 33. Pyell, U.; Jalil, A.H.; Pfeiffer, C.; Pelaz, B.; and Parak, W.J. (2015). Characterisation of gold nanoparticles with different hydrophilic coatings via capillary electrophoresis and Taylor dispersion analysis. Part I: Determination of the zeta potential employing a modified analytic approximation. *Journal of Colloid and Interface Science*, 450, 288-300.
- 34. Bettersize Instruments Ltd. (2023). Characterising zeta potential and distribution of battery electrode slurry averages. Retrieved October 6, 2024, from https://www.azom.com/article.aspx?ArticleID=22912.
- 35. Sikora, A.; Shard, A.G.; and Minelli, C. (2016). Size and ζ-potential measurement of silica nanoparticles in serum using tunable resistive pulse sensing. *Langmuir*, 32(9), 2216-2224.